Rosenbluth Separation of the π^0 Electroproduction Cross Section

M. Defurne,[1,†] M. Mazouz,[2] Z. Ahmed,[3] H. Albataineh,[4] K. Allada,[5] K. A. Aniol,[6] V. Bellini,[7] M. Benali,[8] W. Boeglin,[9] P. Bertin,[8,10] M. Brossard,[8] A. Camsonne,[10] M. Canan,[11] S. Chandavar,[12] C. Chen,[13] J.-P. Chen,[10] C. W. de Jager,[10,*] R. de Leo,[14] C. Desnault,[15] A. Deur,[10] L. El Fassi,[16] R. Ent,[10] D. Flay,[17] M. Friend,[18] E. Fuchey,[8] S. Frullani,[19] F. Garibaldi,[19] D. Gaskell,[10] A. Giusa,[7] O. Glamazdin,[20] S. Golge,[21] J. Gomez,[10] O. Hansen,[10] D. Higinbotham,[10] T. Holmstrom,[22] T. Horn,[23] J. Huang,[5] M. Huang,[24] G. M. Huber,[41] C. E. Hyde,[11,8] S. Iqbal,[6] F. Itard,[8] Ho. Kang,[25] Hy. Kang,[25] A. Kelleher,[26] C. Keppel,[10] S. Koirala,[11] I. Korover,[27] J. J. LeRose,[10] R. Lindgren,[28] E. Long,[29] M. Magne,[8] J. Mammei,[30] D. J. Margaziotis,[6] P. Markowitz,[9] A. Martí Jiménez-Argüello,[31,15] F. Meddi,[19] D. Meekins,[10] R. Michaels,[10] M. Mihovilovic,[32] N. Muangma,[5] C. Muñoz Camacho,[8,15] P. Nadel-Turonski,[10] N. Nuruzzaman,[13] R. Paremuzyan,[15] A. Puckett,[33] V. Punjabi,[34] Y. Qiang,[10] A. Rakhman,[3] M. N. H. Rashad,[11] S. Riordan,[35] J. Roche,[12] G. Russo,[7] F. Sabatié,[1] K. Saenboonruang,[28,36] A. Saha,[10,*] B. Sawatzky,[10,17] L. Selvy,[29] A. Shahinyan,[37] S. Sirca,[32] P. Solvignon,[10,*] M. L. Sperduto,[7] R. Subedi,[38] V. Sulkosky,[5] C. Sutera,[7] W. A. Tobias,[28] G. M. Urciuoli,[39] D. Wang,[28] B. Wojtsekhowski,[10] H. Yao,[17] Z. Ye,[28] L. Zana,[3] X. Zhan,[40] J. Zhang,[10] B. Zhao,[26] Z. Zhao,[28] X. Zheng,[28] and P. Zhu[28]

(Jefferson Lab Hall A Collaboration)

[1]*Irfu, CEA, Université Paris-Saclay, 91191 Gif-sur-Yvette, France*
[2]*Faculté des sciences de Monastir, 5000 Tunisia*
[3]*Syracuse University, Syracuse, New York 13244, USA*
[4]*Texas A&M University-Kingsville, Kingsville, Texas 78363, USA*
[5]*Massachusetts Institute of Technology, Cambridge, Massachusetts 02139, USA*
[6]*California State University, Los Angeles, Los Angeles, California 90032, USA*
[7]*INFN/Sezione di Catania, 95125 Catania, Italy*
[8]*Clermont Université, Université Blaise Pascal, CNRS/IN2P3, Laboratoire de physique corpusculaire, FR-63000 Clermont-Ferrand, France*
[9]*Florida International University, Miami, Florida 33199, USA*
[10]*Thomas Jefferson National Accelerator Facility, Newport News, Virginia 23606, USA*
[11]*Old Dominion University, Norfolk, Virginia 23529, USA*
[12]*Ohio University, Athens, Ohio 45701, USA*
[13]*Hampton University, Hampton, Virginia 23668, USA*
[14]*Università di Bari, 70121 Bari, Italy*
[15]*Institut de Physique Nucléaire CNRS-IN2P3, Orsay 91400, France*
[16]*Rutgers, The State University of New Jersey, Piscataway, New Jersey 08854, USA*
[17]*Temple University, Philadelphia, Pennsylvania 19122, USA*
[18]*Carnegie Mellon University, Pittsburgh, Pennsylvania 15213, USA*
[19]*INFN/Sezione Sanità, 00161 Roma, Italy*
[20]*Kharkov Institute of Physics and Technology, Kharkov 61108, Ukraine*
[21]*North Carolina Central University, Durham, North Carolina 27701, USA*
[22]*Longwood University, Farmville, Virginia 23909, USA*
[23]*The Catholic University of America, Washington, DC 20064, USA*
[24]*Duke University, Durham, North Carolina 27708, USA*
[25]*Seoul National University, Seoul 151-747, South Korea*
[26]*College of William and Mary, Williamsburg, Virginia 23187, USA*
[27]*Tel Aviv University, Tel Aviv 69978, Israel*
[28]*University of Virginia, Charlottesville, Virginia 22904, USA*
[29]*Kent State University, Kent, Ohio 44242, USA*
[30]*University of Massachusetts, Amherst, Massachusetts 01003, USA*
[31]*Facultad de Física, Universidad de Valencia, Valencia 46071, Spain*
[32]*University of Ljubljana, 1000 Ljubljana, Slovenia*
[33]*Los Alamos National Laboratory, Los Alamos, New Mexico 87545, USA*
[34]*Norfolk State University, Norfolk, Virginia 23529, USA*
[35]*Stony Brook University, Stony Brook, New York 11794, USA*
[36]*Kasetsart University, Chatuchak, Bangkok, 10900, Thailand*
[37]*Yerevan Physics Institute, Yerevan 375036, Armenia*
[38]*George Washington University, Washington, DC 20052, USA*

[39]INFN/Sezione di Roma, 00185 Roma, Italy
[40]Argonne National Laboratory, Lemont, Illinois 60439, USA
[41]University of Regina, Regina, Saskatchewan S4S 0A2, Canada

(Received 27 July 2016; revised manuscript received 3 October 2016; published 23 December 2016)

We present deeply virtual π^0 electroproduction cross-section measurements at $x_B = 0.36$ and three different Q^2 values ranging from 1.5 to 2 GeV^2, obtained from Jefferson Lab Hall A experiment E07-007. The Rosenbluth technique is used to separate the longitudinal and transverse responses. Results demonstrate that the cross section is dominated by its transverse component and, thus, is far from the asymptotic limit predicted by perturbative quantum chromodynamics. Nonetheless, an indication of a nonzero longitudinal contribution is provided by the measured interference term σ_{LT}. Results are compared with several models based on the leading-twist approach of generalized parton distributions (GPDs). In particular, a fair agreement is obtained with models in which the scattering amplitude includes convolution terms of chiral-odd (transversity) GPDs of the nucleon with the twist-3 pion distribution amplitude. This experiment, together with previous extensive unseparated measurements, provides strong support to the exciting idea that transversity GPDs can be accessed via neutral pion electroproduction in the high-Q^2 regime.

DOI: 10.1103/PhysRevLett.117.262001

Deep exclusive reactions have been the subject of intense experimental and theoretical work in the past decades, as they provide clean probes of the internal three-dimensional structure of hadrons. We present here measurements of the differential cross section for the forward exclusive electroproduction reaction $ep \to ep\pi^0$. These results are the first separation of the differential cross section for longitudinally and transversely polarized virtual photons of exclusive π^0 electroproduction in the electron-scattering kinematics of deep inelastic scattering (DIS). A diagram of this process, including definitions of the kinematic variables, is presented in Fig. 1.

The quantum chromodynamics (QCD) factorization theorems predict that deep virtual meson production should be dominated by the longitudinal virtual photoproduction cross section [1]. In the Bjorken limit $Q^2 \to \infty$ and $t/Q^2 \ll 1$ at fixed x_B, the longitudinal scattering amplitude factorizes into a hard perturbative contribution, the leading-twist generalized parton distributions (GPDs) of the nucleon and the pion distribution amplitude (DA) [1–3]. GPDs describe the three-dimensional structure of hadrons by correlating the internal transverse position of partons to their longitudinal momentum [4–6]. In the case of a nucleon and at leading twist, four chiral-even GPDs conserve the helicity of the parton, whereas four chiral-odd GPDs, also referred to as transversity GPDs, flip its helicity. While a rigorous factorization proof has not been established for the transverse virtual photoproduction amplitude, it is proven to be suppressed by a factor of $1/Q$ with respect to its longitudinal counterpart [1].

The leading-twist approximation is in good agreement with high-Q^2 electroproduction data for photon [7–9] and vector meson production [10,11]. On the other hand, the collinear approximation underestimates by about one order of magnitude the total π^0 electroproduction cross sections measured at $Q^2 \simeq 2$ GeV^2 by the Hall A [12] and CLAS [13,14] Collaborations at Jefferson Lab (JLab). It was suggested in Refs. [15,16] that for neutral meson production the twist-3 quark-helicity flip pion DAs coupled with the transversity GPDs of the proton would create a large cross section for transversely polarized virtual photons, without violating the QCD factorization theorem. These calculations are in good agreement (within model uncertainties) with the unseparated cross sections of Refs. [13,14]. The present study is undertaken to verify whether or not the separated cross sections for longitudinally and transversely polarized virtual photons can be accurately described by a formalism based on leading-twist GPDs.

The deeply virtual meson production cross section can be written in the following form [17]:

$$\frac{d^4\sigma}{dQ^2 dx_B dt d\phi} = \frac{1}{2\pi}\frac{d^2\Gamma}{dx_B dQ^2}(Q^2, x_B, E)\left(\frac{d\sigma_T}{dt} + \epsilon\frac{d\sigma_L}{dt} + \sqrt{2\epsilon(1+\epsilon)}\frac{d\sigma_{TL}}{dt}\cos\phi + \epsilon\frac{d\sigma_{TT}}{dt}\cos 2\phi\right), \quad (1)$$

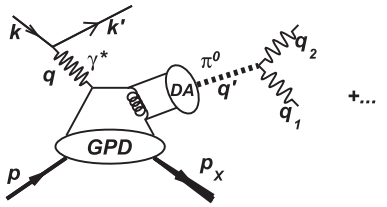

Invariants
$Q^2 = -(k-k')^2$
$x_B = Q^2/(2q\cdot P)$
$W^2 = (q+P)^2$
$t = (q-q')^2$

FIG. 1. Diagram of the exclusive π^0 electroproduction reaction, identified by the $\pi^0 \to \gamma\gamma$ decay mode. The value of t with minimal $|t|$ can be evaluated as $t_{\min} = (Q^2 + m_\pi^2)^2/(4W^2) - (|q^{\text{c.m.}}| - |q'^{CM}|)^2$, with $|q^{\text{c.m.}}|$ and $|q'^{CM}|$ the norms of $\vec{q}$ and $\vec{q}'$, respectively, in the $p\pi^0$ final state center-of-mass frame.

TABLE I. E07-007 $ep \to ep\pi^0$ kinematic settings.

Setting	Q^2 (GeV^2)	x_B	E^{beam} (GeV)	ϵ
Kin1	1.50	0.36	3.355	0.52
			5.55	0.84
Kin2	1.75	0.36	4.455	0.65
			5.55	0.79
Kin3	2.00	0.36	4.455	0.53
			5.55	0.72

where E is the incident lepton energy in the target rest frame and ϕ the angle between the leptonic and hadronic plane defined according to the Trento convention [18]. The factor $(d^2\Gamma/dx_B dQ^2)(Q^2, x_B, E)$ is the virtual photon flux, and ϵ is the degree of longitudinal polarization defined as $(y = [q \cdot P]/[k \cdot P])$:

$$\frac{d^2\Gamma}{dx_B dQ^2}(Q^2, x_B, E) = \frac{\alpha}{8\pi}\frac{Q^2}{M^2E^2}\frac{1-x_B}{x_B^3}\frac{1}{1-\epsilon}, \quad (2)$$

$$\epsilon = \frac{1 - y - Q^2/4E^2}{1 - y + y^2/2 + Q^2/(4E^2)}, \quad (3)$$

M being the proton mass.

Experiment E07-007 ran in JLab Hall A from October to December, 2010. One of its goals was to separate the exclusive transverse and longitudinal π^0 electroproduction cross sections using the Rosenbluth technique, consisting of measurements at two different values of the incident electron energy at each setting. Table I lists the three Q^2 settings measured, each of them at two different values of ϵ.

The electron beam was incident on a 15-cm-long liquid H_2 target, for a typical luminosity of 2×10^{37} cm^{-2} s^{-1}. Scattered electrons were detected in a high resolution spectrometer (HRS), with 10^{-4} momentum resolution and better than 2 mr horizontal angular resolution [19]. The two photons of the π^0 decays were detected in a PbF_2 electromagnetic calorimeter consisting of a 13×16 array of $3 \times 3 \times 18.6$ cm^3 crystals, coupled to mesh-dynode photomultipliers. Each calorimeter channel was continuously sampled by a 1 GHz flash Analog-to-Digital converter system that recorded the signal over 128 ns. The high resolution in the electron kinematics accurately determined the event-by-event (Q^2, x_B) values. The fast Cherenkov signal from the calorimeter allowed a coincident time resolution between the electron and π^0 detections of 0.6 ns. The vertex resolution of the HRS and position resolution of the calorimeter accurately determined the π^0 direction and thus the kinematical variables t and ϕ. The measured energy in the calorimeter is used to identify π^0 events through the two-photon invariant mass $m_{\gamma\gamma} = \sqrt{(q_1 + q_2)^2}$ and to ensure the exclusivity of the reaction using the $ep \to e\gamma\gamma X$ missing mass squared $M^2_{ep\to e\gamma\gamma X}$.

The calibration of the calorimeter was done in two steps. First, we used elastic scattering $H(e, e'_{\text{Calo}} p_{\text{HRS}})$ events. This calibration required dedicated runs, since the polarity of the HRS had to be reversed to allow proton detection. We performed elastic calibrations at the beginning, middle, and end of the experiment. A resolution of 3.1% at 3.16 GeV was measured, with a position resolution of 3 mm at 110 cm from the target. Between elastic calibrations, channel gains were observed to drift up to 10%. We attributed these changes to radiation damage of the PbF_2 crystals. In order to correct for the calibration coefficient drifts between the elastic run periods, we used exclusive π^0 data from our $H(e, e'\gamma\gamma)X$ sample. By assuming $M^2_{ep\to e\gamma\gamma X} = M^2$ and $m_{\gamma\gamma} = m_{\pi^0}$, the sum of the energies of the two decay photons was determined and used to compute the calibration coefficients. The combination of both elastic and exclusive π^0 calibrations provided a continuous invariant mass resolution of 9.5 MeV through the full run period.

The data acquisition was triggered by an electron detection signal in the HRS, formed by the coincidence of the gas Cherenkov detector and the plastic scintillator plane S2m of the HRS [19]. In order to select neutral pions, we studied two-cluster events in the calorimeter with an energy deposit larger than 500 MeV in each cluster and within 3 ns of the electron detection. To account for the natural correlation between the measured $M^2_{ep\to e\gamma\gamma X}$ and $m_{\gamma\gamma}$ values, we define a corrected missing mass squared:

$$M_X^2 = M^2_{ep\to e\gamma\gamma X} + C \times (m_{\gamma\gamma} - m_{\pi^0}), \quad (4)$$

with the empirical value $C = 12$ GeV. Figure 2 shows the M_X^2 distribution of the $H(e, e'\gamma\gamma)X$ events. Exclusive events are selected by requiring $100 < m_{\gamma\gamma} < 170$ MeV and $M_X^2 < 0.95$ GeV^2. Contamination from the diffractive $ep \to ep\omega$ reaction with a 8.5% branching-ratio $\omega \to \pi^0\gamma$

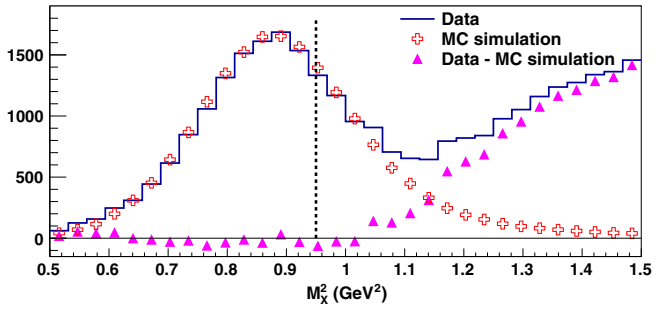

FIG. 2. Distribution of the $H(e, e'\gamma\gamma)X$ events within cuts for Kin3 at $E^{\text{beam}} = 5.55$ GeV and $t_{\min} - t < 0.15$ GeV^2. The Monte Carlo (MC) simulation is represented by the open crosses, whereas the triangles show the estimated inclusive yield obtained by subtracting the simulation from the data. The vertical dotted line illustrates the $M_X^2 < 0.95$ GeV^2 cut applied in the analysis.

decay was estimated to be smaller than 0.3% within our acceptance and cuts based on the measurements performed in Ref. [20]. The inclusive yield obtained by subtracting the simulation from the data is below 2% for $M_X^2 < 0.95$ GeV^2 and treated as a point-to-point systematic uncertainty. The number of accidental $H(e,e'\gamma\gamma)X$ triple coincidences is estimated by measuring the number of two-photon events detected in the calorimeter for each of the three possible timings with respect to the scattered electron: one photon in time and one out of time, both out of time but in time between themselves, and both out of time with the electron and with each other. Finally, an analysis of three-cluster events was performed in order to correct for the fraction of exclusive π^0 events where one of the three clusters was an accidental photon coincidence. This correction was applied bin by bin and found to be 5% on average.

The different terms of the unpolarized π^0 cross section are extracted by minimizing the following χ^2 defined between the number of experimental and simulated events:

$$\chi^2 = \sum_{i=0}^{N} \left(\frac{N_i^{\rm exp} - N_i^{\rm sim}}{\sigma_i^{\rm exp}} \right)^2, \tag{5}$$

where the sum runs over all experimental bins of one Q^2 setting, including data at two different values of ϵ. The variable $N_i^{\rm exp}$ is the number of events in the experimental bin i, with $\sigma_i^{\rm exp}$ being its corresponding uncertainty. The number of simulated events $N_i^{\rm sim}$ is given by

$$N_i^{\rm sim} = \mathcal{L} \int_i \frac{d\sigma}{dt dQ^2 dx_B d\phi} dt dQ^2 dx_B d\phi, \tag{6}$$

with $\mathcal{L}$ the experimental integrated luminosity, corrected by the data acquisition dead time. The integration is performed with a MC simulation, convoluting the known kinematical dependences of the cross section with the experimental acceptance. We limit the analysis to the overlapping $(Q^2;x_B)$-phase space between the two beam-energy settings. After minimization of Eq. (5), the unknown Q^2 dependences of $d\sigma_T/dt$, $d\sigma_L/dt$, $d\sigma_{TT}/dt$, and $d\sigma_{TL}/dt$ are fitted to the results and included into the MC simulation in order to account for the leading variations of the cross section within bins. A second χ^2 minimization is performed, which provides stable results over further iterations and yields the final results we present herein, with $\chi^2/\text{d.o.f.} = 76/60$, $83/80$, and $61/60$, respectively, for $Q^2 = 1.5$, 1.75, and 2.0 GeV^2. No Q^2 dependence is included for $d\sigma_L/dt$, as results are found compatible with zero in all experimental bins. Table II shows the Q dependences obtained. The small HRS acceptance does not allow for an x_B-dependence study.

The Monte Carlo (MC) simulation is based on the GEANT4 toolkit. It includes radiative corrections following the procedure described in Ref. [8] based on calculations by Vanderhaeghen *et al.* [21]. A comparison with the radiative calculations of Ref. [22] at our central kinematics showed agreement within 2%. The HRS acceptance is modeled by an R function that defines the distance of the particle from the HRS acceptance bound [23]. Our cut on M_X^2 to ensure exclusivity removes a significant fraction of exclusive π^0 events. This is compensated by applying an identical cut on the simulated data. For this to be accurate, the experimental and MC simulated M_X^2 (and $m_{\gamma\gamma}$) distributions should have exactly the same widths and positions. These parameters are dominated by the calibration and resolution of the electromagnetic calorimeter crystals. Thus, great care was taken to locally reproduce the calorimeter energy and position resolutions in the MC simulation. While the number of π^0 events removed by the M_X^2 cut depends on ϕ and t, its systematic uncertainty was found almost independent of the kinematics, with a value of 2% estimated by varying the applied cut. In order to propagate this point-to-point uncertainty to the extraction of the four structure functions, we added it in quadrature to the statistical uncertainty when computing the $\sigma_i^{\rm exp}$ of each bin in Eq. (5).

TABLE II. Q dependence obtained from the fit of the t-integrated responses, with statistical and systematics uncertainties added in quadrature, by the function $A/Q^{n_{\rm exp}}$. The QCD asymptotic limit of each term is $\sim Q^{-n_{\rm theo}}$.

Term	$n_{\rm exp}$	$n_{\rm theo}$
$d\sigma_T/dt$	9 ± 2	8
$d\sigma_{TT}/dt$	4 ± 2	8
$d\sigma_{TL}/dt$	26 ± 5	7

Table III lists the different sources of correlated systematic uncertainties. A check of our global normalization was made by extracting the DIS cross section in each of our kinematic settings. Results agree within the uncertainty listed in Table III with the parametrization of the DIS cross section in Ref. [24].

Figure 3 presents the electroproduction cross section $2\pi(d^2\sigma/dtd\phi)$ for the three different Q^2 values and the

TABLE III. Normalization systematic uncertainties in the extracted π^0 electroproduction cross sections. They are approximately correlated in ϕ and t.

Systematic uncertainty	Value
HRS acceptance cut	1%
Gas Cherenkov detector efficiency	0.5%
HRS tracking efficiency	0.5%
π^0 detection efficiency	0.5%
Radiative corrections	2%
Dead time and luminosity	2%
Total	3.12%

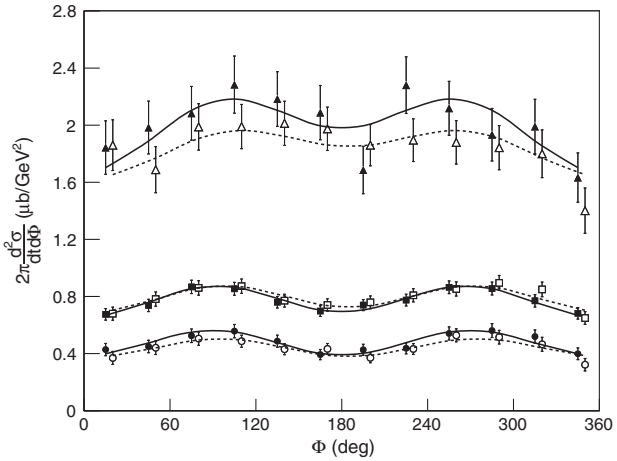

FIG. 3. $2\pi(d^2\sigma/dtd\phi)$ for $Q^2 = 1.5$ (triangles), 1.75 (squares), and 2 GeV^2 (circles) at $x_B = 0.36$ and $t_{\min} - t = 0.025$ GeV^2. The cross sections extracted at low (high) ϵ are shown in open (solid) symbols [and dashed (solid) lines].

lowest $t' = t_{\min} - t$ bin, as a function of ϕ. The cross section is almost independent of ϵ, indicating that most of the signal is coming from its transversely polarized component.

The uncertainties of the Rosenbluth separated $(d\sigma_L/dt)$ and $(d\sigma_T/dt)$ are amplified by the limited lever arm in ϵ and the small ratio $(d\sigma_L/dt)/(d\sigma_T/dt)$. Once the normalization uncertainty is propagated, σ_L is found to be compatible with zero, as seen in Fig. 4. However, the interference cross section $(d\sigma_{TL}/dt)$ is nonzero, which means that $(d\sigma_L/dt)$, though small, is not negligible. The fact that $(d\sigma_T/dt) \gg (d\sigma_L/dt)$ shows that this kinematic regime is still far from the asymptotic prediction of perturbative QCD. These results are compared to previous unseparated measurements at similar kinematics from the Hall A [12] ($Q^2 = 1.9$ GeV^2, $x_B = 0.36$) and CLAS [13,14] ($Q^2 = 2.2$ GeV^2, $x_B = 0.33$) Collaborations. Results are compatible within uncertainties, but the region of direct kinematic overlap is limited to our highest Q^2 setting. Several models are also shown in Fig. 4. The leading-twist chiral-even GPD Vanderhaeghen-Guichon-Guidal (VGG) model [2] predicts a very small longitudinal cross section, compatible with our results. Two models, incorporating both the chiral-even and chiral-odd GPDs, are also shown in Fig. 4 [16,25]. In these models, leading-twist chiral-odd (transversity) GPDs of the nucleon are coupled to a twist-3 DA of the pion, and singularities that otherwise prevent collinear factorization in the case of transversely polarized virtual photons are regularized by the transverse momentum $k_\perp$ of the quarks and antiquarks making up the meson. These models are in good agreement with our results for both $(d\sigma_T/dt)$ and $(d\sigma_L/dt)$ within the experimental uncertainties. However, they predict the opposite sign for

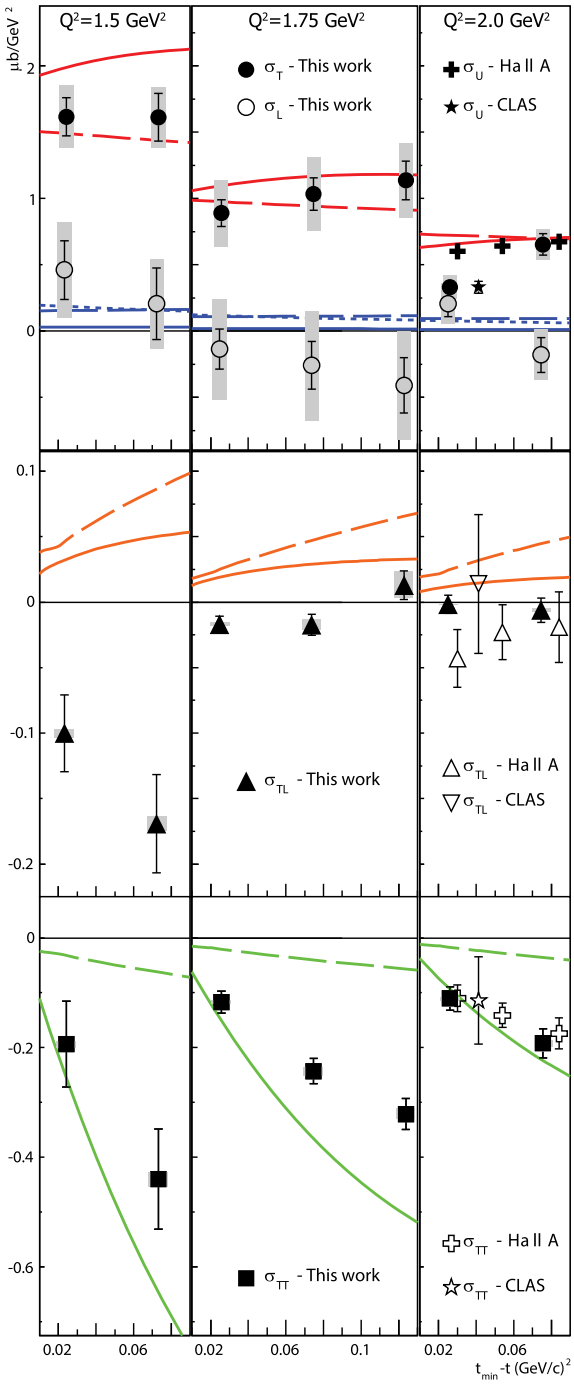

FIG. 4. $d\sigma_T$ (full circles), $d\sigma_L$ (open circles), $d\sigma_{TL}$ (triangles), and $d\sigma_{TT}$ (squares) as a function of $t_{\min} - t$ for $Q^2 = 1.5$ (left), 1.75 (center), and 2 GeV^2 (right) at $x_B = 0.36$. The full lines are predictions from Ref. [16] and the long-dashed lines from Ref. [25]. The short-dashed line show the VGG model [2] for $d\sigma_L$. Solid boxes around the points show normalization systematic uncertainties; for $d\sigma_L$ and $d\sigma_T$, these uncertainties are strongly anticorrelated. Previous unseparated measurements $(\sigma_U = \sigma_T + \epsilon\sigma_L)$ at similar, but not equal, kinematics are also shown and described in the text.

$(d\sigma_{TL}/dt)$ and do not reproduce the Q dependence of the interference terms listed in Table II, especially for σ_{TL}/dt.

In conclusion, we have performed the L/T separation of the π^0 electroproduction cross section for $Q^2 = 1.5$, 1.75, and 2.0 GeV^2 at $x_B = 0.36$. $(d\sigma_L/dt)$, though compatible with zero, is also consistent with the leading-twist predictions of a model of the chiral-even GPDs [2]. We observe fair agreement (particularly at our largest Q^2 kinematic) between these results and two models incorporating transversity GPD. This supports the prediction of a chirally enhanced helicity-flip pion distribution amplitude [15,16] and the exciting possibility of accessing transversity GPDs of the nucleon through exclusive π^0 electroproduction for $Q^2 \geq 1.5$ GeV^2.

We thank G. Goldstein, S. Goloskokov, M. Guidal, P. Kroll, S. Liuti, and M. Vanderhaeghen for valuable information about their work and providing the results of their models. We acknowledge essential work of the JLab accelerator staff and the Hall A technical staff. This work was supported by the Department of Energy (DOE), the National Science Foundation, the French Centre National de la Recherche Scientifique, the Agence Nationale de la Recherche, the Commissariat à l'énergie atomique et aux énergies alternatives, and P2IO Laboratory of Excellence. Jefferson Science Associates, LLC, operates Jefferson Lab for the U.S. DOE under U.S. DOE Contract No. DE-AC05-060R23177.

*Deceased.
†maxime.defurne@cea.fr

[1] J. C. Collins, L. Frankfurt, and M. Strikman, Phys. Rev. D **56**, 2982 (1997).
[2] M. Vanderhaeghen, P. A. M. Guichon, and M. Guidal, Phys. Rev. D **60**, 094017 (1999).
[3] K. Goeke, M. V. Polyakov, and M. Vanderhaeghen, Prog. Part. Nucl. Phys. **47**, 401 (2001).
[4] D. Mueller, D. Robaschik, B. Geyer, F. M. Dittes, and J. Horejsi, Fortschr. Phys. **42**, 101 (1994).
[5] X.-D. Ji, Phys. Rev. Lett. **78**, 610 (1997).
[6] A. V. Radyushkin, Phys. Rev. D **56**, 5524 (1997).
[7] A. Airapetian *et al.* (HERMES Collaboration), J. High Energy Phys. 06 (2008) 066.
[8] M. Defurne *et al.* (Jefferson Lab Hall A Collaboration), Phys. Rev. C **92**, 055202 (2015).
[9] H. S. Jo *et al.* (CLAS Collaboration), Phys. Rev. Lett. **115**, 212003 (2015).
[10] G. Wolf, Rep. Prog. Phys. **73**, 116202 (2010).
[11] L. Favart, M. Guidal, T. Horn, and P. Kroll, Eur. Phys. J. A **52**, 158 (2016).
[12] E. Fuchey *et al.*, Phys. Rev. C **83**, 025201 (2011).
[13] I. Bedlinskiy *et al.* (CLAS Collaboration), Phys. Rev. Lett. **109**, 112001 (2012).
[14] I. Bedlinskiy *et al.* (CLAS Collaboration), Phys. Rev. C **90**, 025205 (2014).
[15] S. Ahmad, G. R. Goldstein, and S. Liuti, Phys. Rev. D **79**, 054014 (2009).
[16] S. Goloskokov and P. Kroll, Eur. Phys. J. A **47**, 112 (2011).
[17] D. Drechsel and L. Tiator, J. Phys. G **18**, 449 (1992).
[18] A. Bacchetta, U. D'Alesio, M. Diehl, and C. A. Miller, Phys. Rev. D **70**, 117504 (2004).
[19] J. Alcorn *et al.*, Nucl. Instrum. Methods Phys. Res., Sect. A **522**, 294 (2004).
[20] L. Morand *et al.* (CLAS Collaboration), Eur. Phys. J. A **24**, 445 (2005).
[21] M. Vanderhaeghen, J. M. Friedrich, D. Lhuillier, D. Marchand, L. Van Hoorebeke, and J. Van de Wiele, Phys. Rev. C **62**, 025501 (2000).
[22] A. Afanasev, I. Akushevich, V. Burkert, and K. Joo, Phys. Rev. D **66**, 074004 (2002).
[23] M. Rvachev, Jefferson Lab, Hall A Technical Note Report No. Jlab-TN-01-055, 2001.
[24] A. Accardi, M. E. Christy, C. E. Keppel, W. Melnitchouk, P. Monaghan, J. G. Morfin, and J. F. Owens, Phys. Rev. D **81**, 034016 (2010).
[25] G. R. Goldstein, J. O. Hernandez, and S. Liuti, Phys. Rev. D **84**, 034007 (2011).